Ferroic Order for Anisotropic Magnetic Dipole Term in Collinear Antiferromagnets of $(t_{2g})^4$ System

Norimasa Sasabe,[1,*] Masaichiro Mizumaki,[1,*] Takayuki Uozumi,[2] and Yuichi Yamasaki[3,4]

[1]*Japan Synchrotron Radiation Research Institute, SPring-8 Kouto, Sayo, Hyogo 679-5198, Japan*
[2]*Graduate School of Engineering, Osaka Metropolitan University, Sakai, Osaka 599-8531, Japan*
[3]*Center for Basic Research on Materials, National Institute for Materials Science (NIMS), Tsukuba, Ibaraki 305-0047, Japan*
[4]*RIKEN Center for Emergent Matter Science (CEMS), Wako, Saitama 351-0198, Japan*

We present the possibility of x-ray magnetic circular dichroism on RuO_2 with collinear antiferromagnetism (AFM). Given that the crystal symmetry breaks the time reversal symmetry when the antiparallel spin aligns along the [100] direction, the expectation vector of the anisotropic magnetic dipole operator $\langle t \rangle$ remains uncanceled along the [010] direction. Our Letter reveals that the magnetic dipole (T_z) term in the x-ray magnetic circular dichroism is induced by the residual $\langle t \rangle$. Because the features of the magnetic moment can be detected via absorption measurements even in the AFM, this technique will be useful for determining the magnetic phase, the Van Vleck–type paramagnet or the excitonic AFM in $(t_{2g})^4$ system.

Spatial inversion and time reversal symmetry (TRS) breaking are the most fundamental information for macroscopic properties in condensed matter physics; the emergence of electric polarization and magnetization leads to spatial inversion and TRS breaking, respectively [1]. Simultaneous spatiotemporal symmetry breaking allows the magnetoelectric effect [2], and is sometimes realized in multiferroic materials [3], where ferroelectric polarization and ferromagnetic magnetization coexist [4]. Symmetry breaking can be detected by using the symmetric feature of the measurement probe. For example, circularly polarized light with breaking the TRS can detect the magnetization, which is known as magnetic circular dichroism (MCD) [5]. However, the existence of magnetization is a sufficient condition, but not a necessary condition for the occurrence of MCD. In other words, the MCD can be allowed even in the absence of magnetization, if the TRS is broken throughout the crystal [6,7].

In recent years, emergent phenomena have been observed in the TRS breaking antiferromagnets with no net magnetization. For example, Mn_3Sn is a 120° antiferromagnetic structure with negative vector chirality on a network of breathing Kagomé lattices, which breaks the TRS. This material has been reported to be a Weyl antiferromagnet, and exhibits the anomalous Hall effect (AHE) and magneto-optical Kerr effect [7–9]. Although Mn_3Sn has a noncollinear magnetic structure of 120°, the AHE derived from TRS breaking has also been theoretically proposed in a collinear antiferromagnet RuO_2 [10,11]. When the antiferromagnetic Néel vector $N = m_2 - m_1$ with magnetic moment m_i of the ith Ru ion is oriented along the [100] direction as shown in Fig. 1(a), the TRS is

broken and the Berry curvature Ω emerges along the [010] direction [10].

X-ray MCD (XMCD) has been theoretically proposed to be possible in a noncollinear antiferromagnet [12–15]. Considering the orbital state frozen from the crystal field and a 120° magnetic structure with negative vector chirality,
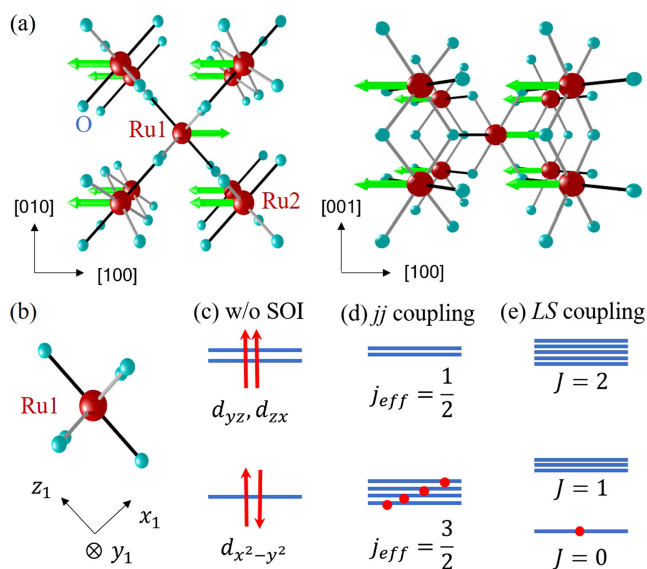

FIG. 1. (a) Crystal and magnetic structure with the Néel vector aligned along the [$\bar{1}$00] direction for the rutile structure. (b) Definition of local coordinates of RuO_6 cluster, and (c) electronic configuration for an intermediate spin state $(t_{2g})^4$ without the spin-orbit interaction (SOI). Two approximation states, i.e., (d) jj coupling and (e) LS coupling, are shown for the electronic state with SOI.

the XMCD originating from the anisotropic magnetic dipole (AMD) order is expressed [13]. The antiferromagnetic structure across multiple magnetic sites is understood as augmented (cluster) multipoles; the magnetic structure is classified as the augmented magnetic octupoles (AMO) [16]. The operator of AMD is not orthogonal to that of AMO, and thus its projection component is detectable in XMCD as the T_z term [17]. Recently, the role of the AMD has attracted much attention, and the relationship between the AMD and AHE has been discussed even for collinear magnetic structures [18]. In this study, we evaluate the possibility of XMCD originating from the T_z term in the collinear antiferromagnet rutile RuO_2 from symmetry arguments and spectral calculations. In particular, we consider the effect of spin-orbit interaction (SOI), which may act more strongly in the $4d$ electron system than in the $3d$ electron system.

The AMD operator t_α ($\alpha = x$, y, z) is expressed as $t_\alpha = \sum_{\beta=x,y,z} Q_{\alpha\beta} s_\beta$, where s and $Q_{\alpha\beta}$ denotes the spin and the electric quadrupole operators, respectively [19,20]. The t_z term depends on the quadrupole moment of the $4d$ orbitals even though the spin moment is the same [21,22]. The quantization axis (QA) of the collinear spin ordered state is often determined as the parallel direction of spin ($s\|z$) and/or incident x-ray wave vector ($k\|z$) [28], whereas a better approach may be to determine the QA of the antiferromagnet by considering the quadrupole moment accompanied by the symmetry of the crystal field due to the electron-lattice interaction [14]. If the magnetic symmetry operation of the antiferromagnetic order does not match that of the crystal, a residual AMD may be allowed, and then the T_z term in XMCD may appear macroscopically. In order to qualitatively understand the collinear antiferromagnets of the $4d^4$ compound RuO_2 [29], we examined (i) the expression of the AMD and the T_z term from the viewpoint of symmetry and (ii) the dependence of the T_z term on the SOI. Moreover, the XMCD spectra are calculated with consideration of the full multiplet effect, and then we discuss the relationship between the AMD and XMCD.

The Ru ion is located in a distorted octahedron with oxygen coordination of local D_{2h} symmetry, as shown in Fig. 1(b). We assume that the local z_1 axis (x_1y_1 plane) is parallel (perpendicular) to the [110] crystalline direction; thus, the electrons occupy the t_{2g} set ($d_{x^2-y^2}/d_{yz}/d_{xz}$) and e_g set ($d_{3z^2-r^2}/d_{xy}$) [30]. Because of competition between the on-site Coulomb exchange of Hund's coupling and the crystal-field splitting (CFS), a strong crystal field favors the low-spin ($S = 0$) or intermediate-spin ($S = 1$) state with $(t_{2g})^4$, whereas the Coulomb exchange favors the high-spin state ($S = 2$) with $(t_{2g})^3(e_g)$. Before discussing RuO_2, we introduce the electronic structure of the $(t_{2g})^4$ state [31]. If the SOI is not taken into account, the four electrons are occupied [32], as shown in Fig. 1(c), where the orbital
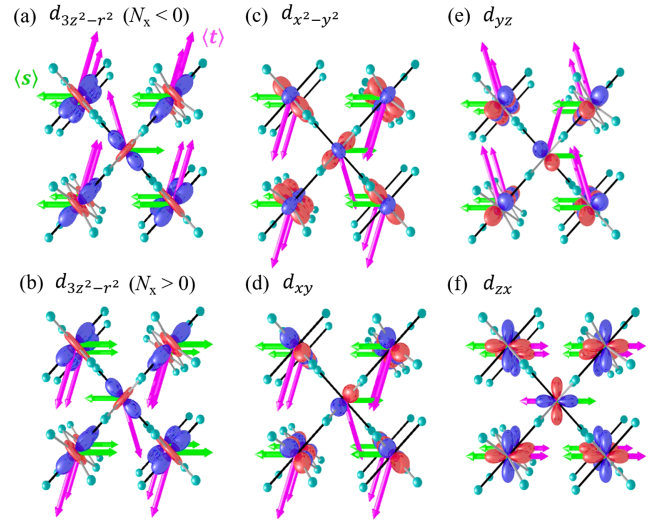

FIG. 2. Anisotropic magnetic dipole operator $\langle t \rangle$ for the collinear antiferromagnet rutile, (a), (b) $d_{3z^2-r^2}$, (c) $d_{x^2-y^2}$, (d) d_{xy}, (e) d_{yz}, and (f) d_{zx} orbitals. The Néel vector is set to [100] for (b) and [$\bar{1}$00] for the other frames.

angular momentum is quenched ($L_z = 0$). In contrast, in the limit of a strong SOI in Fig. 1(d), the t_{2g} orbital splits into $J_{eff} = 1/2$ and $3/2$, and then electrons fully occupy the quartet $J_{eff} = 3/2$ state, resulting in a nonmagnetic $J = 0$ state. Even in the weak SOI case in Fig. 1(e), the SOI makes the nonmagnetic $J = L - S = 0$ state the most stable. Therefore, Ru^{4+} is estimated to be nonmagnetic, but magnetism may be acceptable because of the interatomic interaction, as discussed in detail below.

Figures 2(a) and 2(b) show the collinear antiferromagnetic structures for $d_{3z^2-r^2}$ orbital with $N\|[\bar{1}00]$ and $N\|[100]$, respectively. Considering the quadrupole and direction of the spin moment at each site of antiferromagnetism (AFM) ordered, the AMD moment $\langle t \rangle$ is not completely canceled out and has a ferroic component along the [010] direction; see Sec. I of Supplemental Material [21]. Therefore, the pure T_z term XMCD can be expressed when x rays are irradiated along the [010] direction in the case of $N\|[100]$. By the same argument, $t\|[110]$ is allowed if $N\|[110]$.

The expected t vectors for the different orbitals are shown in Figs. 2(c)–2(f). For the $d_{x^2-y^2}$ and d_{xy} orbitals, there is also a residual t vector along the [0$\bar{1}$0] direction; however, they are in the opposite direction to that for $d_{3z^2-r^2}$. In contrast, the residual t vector of d_{yz} is parallel to the [010] direction. The absolute values of these residual t vectors are the same, whereas the residual t vector of the d_{zx} orbital is zero because the t vectors are antiparallel to the spin moment. In order to study AMD of a multielectron system, we employ the summation of the t vectors ($T^{(ion)} \equiv \sum_\alpha t_\alpha$) at each site and the summation among nonequivalent sites ($T \equiv \sum_i T_i^{(ion)}$; i site). Because $T \neq 0$

is a sufficient condition for emerging XMCD of antiferromagnets, it is necessary to lift the degeneracy due to the crystal field and spin polarization to cause a difference in the up and down spin densities of states at the same time. In the $(t_{2g})^4$ case, where there are two holes in d_{yz} and d_{zx} for the t_{2g} set, as shown in Fig. 1(c), the d_{yz} orbital can solely contribute to T, and the XMCD signal is expected to arise.

In order to discuss the possibility of the XMCD response of RuO$_2$ quantitatively, it is necessary to examine the competition among the three competing interactions, i.e., the CFS, SOI, and interatomic magnetic interaction between Ru1 and Ru2. Therefore, we investigated the features of the simple $(t_{2g})^4$ model within the mean field approximation of interatomic magnetic interaction which is treated as a molecular field (MF). The effective Hamiltonian of the simple $(t_{2g})^4$ model is described as

$$H_{\text{eff}} = \Delta(L_Z)^2 + \lambda \boldsymbol{L} \cdot \boldsymbol{S} - g_J \boldsymbol{m} \cdot \boldsymbol{h}_{\text{MF}}, \qquad (1)$$

where Δ, λ, and $g_J \boldsymbol{h}_{\text{MF}}$ are the parameters of the CFS, SOI, and MF, respectively. The t_{2g} levels are set as shown in Fig. 1(c) [32]. The Landé g factor becomes $g_J = 3/2$ because of the LS coupling approximation with $L = S = 1$, and $\boldsymbol{h}_{\text{MF}}$ is assumed to be applied along the z direction of local coordinates in the RuO$_6$ cluster, as shown in Fig. 1(b).

Figure 3(a) shows a phase diagram and the expected value of the total AMD moment $\langle T_z \rangle$ of the $(t_{2g})^4$ electronic state, where the horizontal axis indicates the SOI value normalized by the crystal field, i.e., λ/Δ. The left vertical axis indicates the MF intensity which affect the phase transition of the $(t_{2g})^4$ model, and the right vertical axis shows the $\langle T_z \rangle$ value. At $\lambda = 0$ (the weak SOI limit), the ground state of $(t_{2g})^4$ is the $S = 1$ triple states, and the $S_z = 0$ state contains the basis $J = 0$ of the LS coupling scheme shown in Fig. 1(e). The $S_z = 1$ state contains the basis $J_z = 1$ ($J = 1$) of the LS coupling scheme, and $S_z = -1$ contains $J_z = -1$. The $J = 0$ state, paramagnetism (PM), is the most stable state under a moderate SOI; as the SOI becomes stronger, it soon becomes the nominally nonmagnetic phase, $\tilde{J} = 0$ (Van Vleck–type PM). However, the interatomic magnetic interaction between the excited $J = 1$ states induces the magnetic moment; thus, it splits the $|J, m\rangle$ multiplet by the Zeeman energy $E_{\text{MF}} = -g_J \boldsymbol{m} \cdot \boldsymbol{h}_{\text{MF}}$. Hence, because of the interaction between the excitonic triplets, which are sometimes called a triplon condensation [32] or spin-orbit excitonic antiferromagnet [33–35], the magnetic state, $\tilde{J} = 1$ (excitonic AFM), becomes more stable than the Van Vleck–type PM.

We focus on the $\langle T_z \rangle$ values of the $(t_{2g})^4$ model and compare them with those of the Ru^{4+} model which includes CFS and MF terms of the interatomic spin interaction within full multiplet effect of Ru^{4+}; see Supplemental Material, Sec. II [21] and Refs. [23–27]. For the $(t_{2g})^4$ model, the blue and red dotted lines in
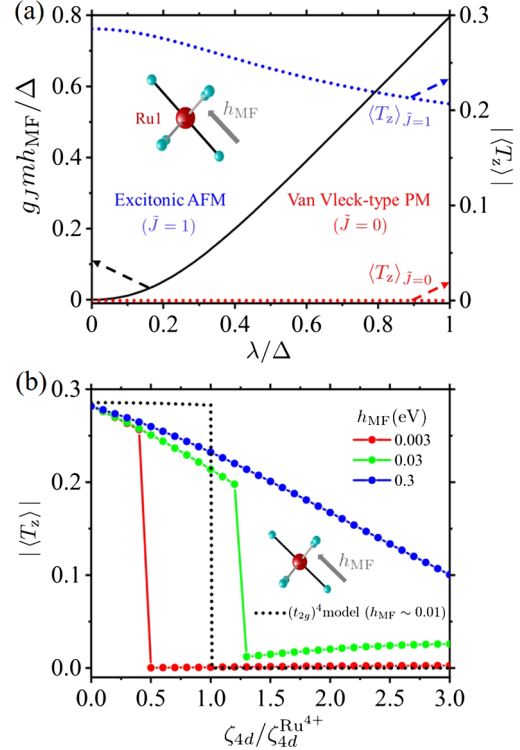

FIG. 3. (a) Phase diagram and $\langle T_z \rangle$ values for the $(t_{2g})^4$ model. The inset shows the direction of h_{MF} on the RuO$_6$ cluster under $\boldsymbol{h}_{\text{MF}} \| \text{QA}$. (b) $\langle T_z \rangle$ value of the Ru^{4+} model. $\langle T_z \rangle$ values are indicated by colored symbols, and the black dotted line indicates the $\langle T_z \rangle$ behavior of the $(t_{2g})^4$ model where $g_J h_{\text{MF}}/\Delta = 0.0118$ when $\lambda/\Delta = 0.1$. ζ_{4d} is the spin-orbit coupling constant for the $4d$ orbital, where the ζ_{4d} value of Ru^{4+} ion ($\zeta_{4d}^{\text{Ru}^{4+}}$) is 0.161 eV.

Fig. 3(a) indicate the $\langle T_z \rangle$ values of the excitonic AFM and Van Vleck–type PM, respectively. With an increase in the SOI parameter λ, the $\langle T_z \rangle$ value of excitonic AFM decreases, while that of the Van Vleck–type PM remains zero. This indicates that measurement of $\langle T_z \rangle$ value can detect the $(t_{2g})^4$ electronic state, where the competition between the two states allows quantum phase transition [36,37]. In order to discuss the electronic state of actual RuO$_2$, the $\langle T_z \rangle$ values of the Ru^{4+} model are simulated, as shown in Fig. 3(b). Here, the red, green, and blue symbols indicate the behavior of the $\langle T_z \rangle$ value depending on the MF intensity. The black dotted line indicates the $\langle T_z \rangle$ values from Fig. 3(a), where the CFS Δ in Eq. (1) is 1.0 eV and that λ is estimated as approximately 0.1 eV in $\zeta_{4d}^{\text{Ru}^{4+}}$. Under this condition, the phase transition between the excitonic AFM and Van Vleck–type PM occurs under $h_{\text{MF}} \sim 0.01$ eV, as shown in Fig. 3(b). From the results for the Ru^{4+} model, as well as the result of the $(t_{2g})^4$ model, the phase transition is observed under weak interatomic magnetic interaction; thus, the electronic states of the Ru^{4+} model are regarded as the excitonic AFM and Van Vleck–type PM. The limited basis set of the $(t_{2g})^4$ model causes a
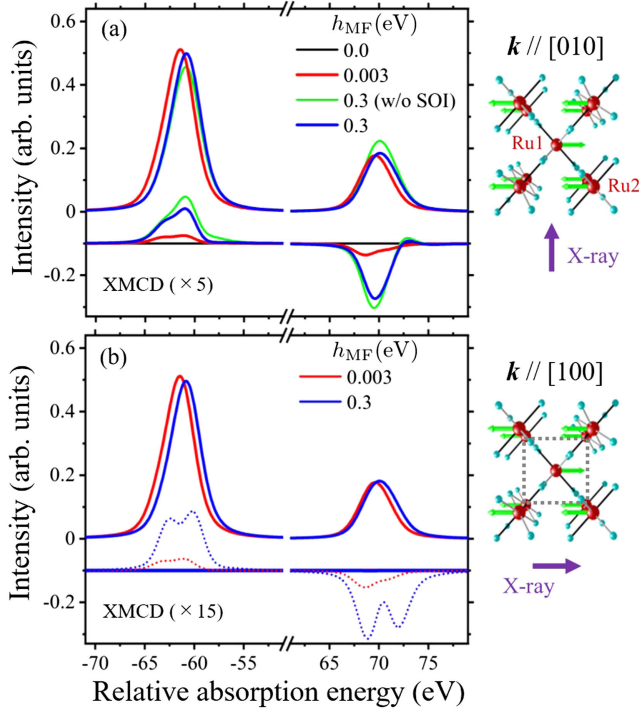
FIG. 4. X-ray absorption spectroscopy (upper result) and XMCD (lower result) spectra around absorption Ru-L edges where (a) $k\|[010]$ and (b) $k\|[100]$: the right (left) structures denote L_{II} (L_{III}).

mild decrease in the $\langle T_z \rangle$ value of excitonic AFM; however, the decrease in the $\langle T_z \rangle$ value of the Ru^{4+} model is larger because the occupation in the e_g set arises from the strengthened SOI. Moreover, for the Ru^{4+} model, the $\langle T_z \rangle$ value becomes nonzero because the intra-atomic spin interaction affects the Van Vleck–type PM. Thus, the electronic state of the Ru^{4+} model with $h_{MF} = 0$ corresponds to a *pure* Van Vleck–type PM.

Figures 4(a) and 4(b) show the results of the spectral calculation by employing the Ru^{4+} model under TRS breaking; the incident x-ray directions in Figs. 4(a) and 4(b) are parallel to [010] and [100], respectively. The upper and lower results in each figure are the x-ray absorption spectra $(\mu^+ + \mu^-)$ and XMCD $(\mu^+ - \mu^-)$, respectively, where μ^+ and μ^- represent the helicities of x rays. The solid lines indicate the total intensity between the Ru1 and Ru2 sites, and the dotted lines in Fig. 4(b) indicate the XMCD intensity on the Ru1 site surrounded by the gray dotted square. We determined the XMCD responses of RuO_2 reflecting the AMD, Van Vleck–type PM (red line) and excitonic AFM (blue line), where the Van Vleck–type PM (excitonic AFM) is $h_{MF} = 0.003$ eV (0.3 eV) with $\zeta_{4d}^{Ru^{4+}}$. The black line in Fig. 4(a) indicates the XMCD simulation of the *pure* Van Vleck–type PM with $\zeta_{4d}^{Ru^{4+}}$, and the green line indicates that of the ideal excitonic AFM with $h_{MF} = 0.3$ and $\zeta_{4d} = 0.0$ (in units of eV). In these calculations, the MF is applied in the [100] direction; thus,

the spin component of Ru1 (Ru2) tends to be parallel along [100] ($[\bar{1}00]$), where the spin direction of Ru1 is antiparallel to that of Ru2 without the SOI ($\zeta_{4d} = 0.0$ eV).

As shown in Fig. 4(a), the XMCD signal is detectable for the excitonic AFM, whereas it is difficult to detect the signal of the Van Vleck–type PM. In contrast, in Fig. 4(b), neither the XMCD signal of the Van Vleck–type PM nor that of the excitonic AFM is observed. This behavior is consistent with the expression for $t\|[010]$ when $N\|[\bar{1}00]$, as shown in Fig. 2; therefore, the AMD is the origin of the XMCD of the RuO_2 collinear antiferromagnetic state, as indicated by the green lines.

The XMCD signal of the excitonic AFM originated from the direction of the AMD moment, which is confirmed in XMCD of Mn_3Sn [38,39]. Focusing on the red line in Fig. 4(a), we discuss the XMCD signal of the Van Vleck–type PM. It is well known that the Van Vleck PM is mixed with the magnetic states when a magnetic field is applied, and then the XMCD signal is observed in the Van Vleck PM under a magnetic field [40]. Therefore, the red line is a reasonable result; this weak XMCD signal results in a canted magnetic moment due to $h_{MF} = 0.003$ eV. Because the XMCD signal arises in both states, the difference between the Van Vleck–type PM and the excitonic AFM is discussed. One clear difference is that the XMCD intensity of the excitonic AFM significantly exceeds that of the Van Vleck–type state, which is affected by the T_z value. In particular, the T_z value of the excitonic AFM is not easily influenced by external magnetic field [38], whereas that of Van Vleck–type PM is sensitive [40]. In addition to the intensity, the XMCD features differ between the excitonic AFM and Van Vleck–type PM; particularly, the structure near 73 eV in L_{II} structure. Thus, investigation of these XMCD spectral features is useful for clarifying the electronic state of RuO_2.

Finally, we discuss the possibility of detecting the XMCD signal and T_z term in actual RuO_2 crystals. It has been reported that the magnetic diffraction at (100) is observed in a bulk crystal RuO_2 by neutron scattering, and the magnetic moment is estimated to be approximately $0.05~\mu_B$ at the ambient temperature [31]. In addition, a resonant x-ray scattering (RXS) study of the Ru L edge in RuO_2 has revealed that the Néel vector is nearly aligned with the c axis [41]. The small magnetic moment suggests that it is close to the Van Vleck PM with moderate spin-orbit coupling, in which the pure XMCD T_z term would not be allowed for the magnetic structure of the bulk RuO_2. Moreover, the XMCD signal of RuO_2 under AFM along the c axis is not observable considering the configuration of the AMO $\langle t \rangle$. Thus, we consider that ferroic T_z is not observed in bulk RuO_2. Instead of ferroic T_z, contribution of the antiferroic T_z term may be included in the RXS spectrum for (100) diffraction, but it is usually difficult to separate from the strong S_z term. In contrast, for the AHE-allowed thin films, the magnetic structures should differ from those in the bulk owing to the change in spin anisotropy caused by the epitaxial strain [42]. Because

the compressive strain strengthens the crystal field, it reduces λ/Δ, resulting in an increase in the excitonic magnetic moment. Conversely, it is expected that tensile strain from the substrate stabilizes the Van Vleck–type PM. This strain control causes a phase transition between the Van Vleck–type PM and excitonic AFM of the $(t_{2g})^4$ system; therefore, our theoretical prediction can be verified by paying attention to the $\langle t \rangle$ behavior or XMCD T_z. In order to estimate the T_z term, we consider that the XMCD sum rule must be carefully applied because of the QA treatment between Ru1 and Ru2. For acquiring the T_z values, theoretical XMCD studies with full multiplet theory are helpful, along with band calculations.

In summary, we theoretically studied how the SOI suppresses the T_z value and XMCD spectra by focusing on the AMD behavior of the collinear antiferromagnetic state of RuO_2. Using the $(t_{2g})^4$ model, we investigated the phase diagram and T_z value of the $(t_{2g})^4$ system, where the phase transition and its quantum states could be controlled by changing the tensile strength. Moreover, XMCD calculations were performed using the Ru^{4+} model based on full multiplet theorem. It was shown that the T_z term is acceptable for lifting orbital degeneracy owing to the crystal field and exchange interaction when the Néel vectors are oriented along the [100] and [110] directions. Because XMCD is detectable in the $\langle t \rangle$ behavior or T_z value of the antiferromagnet, the technique is suitable for evaluating the excitonic (triplon) magnetic moment in the $(t_{2g})^4$ system. The AMD is related to the Berry curvature [18]; thus, spectroscopic and imaging analysis of the AMD through XMCD measurement is a useful method for investigating the AHE and related phenomena [43,44]. Considering the investigations of noncollinear Mn_3Sn and the present XMCD study on collinear RuO_2, we expect that studying the $\langle t \rangle$ behavior is key to understanding new AHE materials and developing functional devices.

[*] Present address: Faculty of Science, Kumamoto University, Kumamoto 860-8555, Japan.

[1] W. Eerenstein, N. Mathur, and J. F. Scott, Nature (London) **442**, 759 (2006).

[2] M. Fiebig, J. Phys. D **38**, R123 (2005).

[3] M. Fiebig, T. Lottermoser, D. Meier, and M. Trassin, Nat. Rev. Mater. **1**, 1 (2016).

[4] Y. Yamasaki, S. Miyasaka, Y. Kaneko, J.-P. He, T. Arima, and Y. Tokura, Phys. Rev. Lett. **96**, 207204 (2006).

[5] P. Stephens, Annu. Rev. Phys. Chem. **25**, 201 (1974).

[6] T. Sato, N. Abe, S. Kimura, Y. Tokunaga, and T.-h. Arima, Phys. Rev. Lett. **124**, 217402 (2020).

[7] T. Higo, H. Man, D. B. Gopman, L. Wu, T. Koretsune, O. M. van't Erve, Y. P. Kabanov, D. Rees, Y. Li, M.-T. Suzuki *et al.*, Nat. Photonics **12**, 73 (2018).

[8] S. Nakatsuji, N. Kiyohara, and T. Higo, Nature (London) **527**, 212 (2015).

[9] M. Ikhlas, T. Tomita, T. Koretsune, M.-T. Suzuki, D. Nishio-Hamane, R. Arita, Y. Otani, and S. Nakatsuji, Nat. Phys. **13**, 1085 (2017).

[10] L. Šmejkal, R. González-Hernández, T. Jungwirth, and J. Sinova, Sci. Adv. **6**, eaaz8809 (2020).

[11] L. Šmejkal, J. Sinova, and T. Jungwirth, Phys. Rev. X **12**, 040501 (2022).

[12] S. Wimmer, S. Mankovsky, J. Minár, A. N. Yaresko, and H. Ebert, Phys. Rev. B **100**, 214429 (2019).

[13] Y. Yamasaki, H. Nakao, and T. hisa Arima, J. Phys. Soc. Jpn. **89**, 083703 (2020).

[14] N. Sasabe, M. Kimata, and T. Nakamura, Phys. Rev. Lett. **126**, 157402 (2021).

[15] G. van der Laan, Phys. Rev. B **104**, 094414 (2021).

[16] M.-T. Suzuki, T. Koretsune, M. Ochi, and R. Arita, Phys. Rev. B **95**, 094406 (2017).

[17] H. Kusunose, R. Oiwa, and S. Hayami, J. Phys. Soc. Jpn. **89**, 104704 (2020).

[18] S. Hayami and H. Kusunose, Phys. Rev. B **103**, L180407 (2021).

[19] J. Stöhr, J. Magn. Magn. Mater. **200**, 470 (1999).

[20] T. Oguchi and T. Shishidou, Phys. Rev. B **70**, 024412 (2004).

[21] See Supplemental Material at http://link.aps.org/supplemental/10.1103/PhysRevLett.131.216501 for details of the anisotropic magnetic dipole operator and the employed Hamiltonian, which includes Refs. [22–27].

[22] J. Stöhr, J. Electron Spectrosc. Relat. Phenom. **75**, 253 (1995).

[23] R. D. Cowan, *The Theory of Atomic Structure and Spectra* (University of California Press, Berkeley, 1981), Vol. 3.

[24] K. Okada and A. Kotani, J. Phys. Soc. Jpn. **58**, 2578 (1989).

[25] A. Tanaka and T. Jo, J. Phys. Soc. Jpn. **61**, 2040 (1992).

[26] M. Taguchi, T. Uozumi, and A. Kotani, J. Phys. Soc. Jpn. **66**, 247 (1997).

[27] M. Matsubara, T. Uozumi, A. Kotani, Y. Harada, and S. Shin, J. Phys. Soc. Jpn. **69**, 1558 (2000).

[28] J. Crocombette, B. Thole, and F. Jollet, J. Phys. Condens. Matter **8**, 4095 (1996).

[29] Z. Hu, H. von Lips, M. S. Golden, J. Fink, G. Kaindl, F. M. F. de Groot, S. Ebbinghaus, and A. Reller, Phys. Rev. B **61**, 5262 (2000).

[30] C. A. Occhialini, V. Bisogni, H. You, A. Barbour, I. Jarrige, J. F. Mitchell, R. Comin, and J. Pelliciari, Phys. Rev. Res. **3**, 033214 (2021).

[31] T. Berlijn, P. C. Snijders, O. Delaire, H.-D. Zhou, T. A. Maier, H.-B. Cao, S.-X. Chi, M. Matsuda, Y. Wang, M. R. Koehler *et al.*, Phys. Rev. Lett. **118**, 077201 (2017).

[32] C. Svoboda, M. Randeria, and N. Trivedi, Phys. Rev. B **95**, 014409 (2017).

[33] G. Khaliullin, Phys. Rev. Lett. **111**, 197201 (2013).

[34] N. Kaushal, R. Soni, A. Nocera, G. Alvarez, and E. Dagotto, Phys. Rev. B **101**, 245147 (2020).

[35] T. Feldmaier, P. Strobel, M. Schmid, P. Hansmann, and M. Daghofer, Phys. Rev. Res. **2**, 033201 (2020).

[36] A. Jain, M. Krautloher, J. Porras, G. Ryu, D. Chen, D. Abernathy, J. Park, A. Ivanov, J. Chaloupka, G. Khaliullin, B. Keimer, and B. Kim, Nat. Phys. **13**, 633 (2017).

[37] S. Kunkemöller, D. Khomskii, P. Steffens, A. Piovano, A. A. Nugroho, and M. Braden, Phys. Rev. Lett. **115**, 247201 (2015).

[38] M. Kimata, N. Sasabe, K. Kurita, Y. Yamasaki, C. Tabata, Y. Yokoyama, Y. Kotani, M. Ikhlas, T. Tomita, K. Amemiya, H. Nojiri, S. Nakatsuji, T. Koretsune, H. Nakao, T.-h. Arima, and T. Nakamura, Nat. Commun. **12**, 5582 (2021).

[39] S. Sakamoto, T. Higo, M. Shiga, K. Amemiya, S. Nakatsuji, and S. Miwa, Phys. Rev. B **104**, 134431 (2021).

[40] S. Agrestini, C.-Y. Kuo, K. Chen, Y. Utsumi, D. Mikhailova, A. Rogalev, F. Wilhelm, T. Förster, A. Matsumoto, T. Takayama, H. Takagi, M. W. Haverkort, Z. Hu, and L. H. Tjeng, Phys. Rev. B **97**, 214436 (2018).

[41] Z. H. Zhu, J. Strempfer, R. R. Rao, C. A. Occhialini, J. Pelliciari, Y. Choi, T. Kawaguchi, H. You, J. F. Mitchell, Y. Shao-Horn, and R. Comin, Phys. Rev. Lett. **122**, 017202 (2019).

[42] Y. Yokoyama, Y. Yamasaki, M. Taguchi, Y. Hirata, K. Takubo, J. Miyawaki, Y. Harada, D. Asakura, J. Fujioka, M. Nakamura, H. Daimon, M. Kawasaki, Y. Tokura, and H. Wadati, Phys. Rev. Lett. **120**, 206402 (2018).

[43] S. Nakatsuji and R. Arita, Annu. Rev. Condens. Matter Phys. **13**, 119 (2022).

[44] L. Šmejkal, J. Sinova, and T. Jungwirth, Phys. Rev. X **12**, 031042 (2022).